Metals and Materials International (2023) 29:457–466
https://doi.org/10.1007/s12540-022-01224-6

Improvement of Bondability by Addition of Carboxylic Acid to the Sinter-Bonding Paste Containing Bimodal-Sized Cu Particles and Rapid Bonding in Air

Doyeop Namgoong[1] · Kim S. Siow[2] · Jong-Hyun Lee[1]

Received: 30 December 2021 / Accepted: 12 April 2022 / Published online: 3 June 2022
© The Author(s) under exclusive licence to The Korean Institute of Metals and Materials 2022

Abstract
Die attachment by pressure (2 MPa)-assisted sinter bonding in air at 300 °C was rapidly achieved using bimodal-sized (1.86 µm and 340 nm) Cu particles, yielding a joint sustainable even at high temperature for wide-band-gap semiconductor-based power devices. Adding carboxylic acid (succinic acid and ascorbic acid) to a used reducing solvent enhanced in situ reducibility during the bonding, which considerably shortened the bonding time required for achieving shear strengths exceeding 15 MPa. The dies bonded for 1 min exhibited shear strengths of 16.0–17.5 MPa, while 5-min-long bonding yielded a nearly full dense bondline structure. The addition of these carboxylic acids delayed the oxidation of Cu particles and reduced the intrinsic oxide layers on the Cu particles more effectively to rapidly form the dense bondline and increase the joint strength.

Keywords Bimodal Cu particle · Sinter bondability · Carboxylic acid · In situ reduction · Shear strength

1 Introduction

Wide-band-gap (WBG) semiconductors continue to replace silicon semiconductors because of their high-power conversion efficiency by low switching loss, high switching frequency, high power capacity, and high breakdown voltage [1–5]. The two most common WBG, i.e., silicon carbide (SiC) and gallium nitride (GaN), are actively developed as the next-generation power devices for applications in electronic vehicles, aircraft, space exploration, and underground well logging [2–7]. In these applications, the power devices may be subjected to high temperatures, as high as 600 °C, which severely limit the use of Pb or Sn-based solders for bonding [1,2,6.7].

Another possible alternative bonding technology is the transient liquid-phase sintering (TLPS) method which transforms the solders alloys into intermetallic compounds with a high melting point as the joining materials [8, 9]. However, TLPS does not overcome reliability issues associated with the formed bondlines because of the irregular voids created by the volume shrinkage phenomenon and inherent brittleness of the intermetallic compounds [8, 9].

Hence, the metallic sinter-bonding method emerges as a viable bonding technology to replace the solder-based methods because of the significantly higher melting temperature than the bonding temperature. In essence, the sintering steps transform the metallic particles with high surface energies into bulk metallic structures, without going through the melting stage, during the bonding process [10–33].

Here, silver (Ag) emerges as the preferred choice of metal particle because of the ease of sintering (reduced oxidation) and handling, the relatively ductile joint, and high thermal conductivity of the formed joints [10–12]. Recent innovations include sinter-bonding techniques that use micrometer-sized or flake-like particles and pressure-less process to ease the joint formation [11, 12]. However, the Ag's high material cost and electrochemical migration characteristics represents significant roadblock in wider industrial adoption of this sintered Ag joint.

Recently, copper (Cu) has garnered increasing attention as a low-cost sinter-bonding material despite its susceptibility

✉ Jong-Hyun Lee
pljh@snut.ac.kr

[1] Department of Materials Science and Engineering, Seoul National University of Science and Technology, Seoul 01811, Republic of Korea

[2] Institute of Micro-Engineering and Nanoelectronics, Universiti Kebangsaan Malaysia, Bangi 43600, Malaysia

to oxidation [12–33]. Several strategies have been adopted to manage this oxidation during the paste formulation and bonding. The most common strategy adopted the vacuum or inert atmosphere to reduce oxidation during the sinter bonding [14–16]. Others suggested the more aggressive methods, such as, using the reducing atmosphere or reductant to eliminate native copper oxides and accelerate the sintering steps [17–33]. The wider adoption and commercialization of sintered Cu joints also depends on the availability of suitable process parameters, i.e., the relationship between the "iron-triangle" parameter sintering pressure, time and temperature [24]. It is expected that Cu sintering will take a longer duration than Ag sintering of equivalent sintering temperature and pressure to compensate for the ease of Cu oxidation and the higher melting point of Cu compared to Ag.

In terms of the fast sinter bonding process, the 5-min-long pressure-assisted bonding in various atmospheres can be considered a representative process time [14, 17, 28]. Nevertheless, a consistent reduction in the bonding time is always targeted at the power electronic and electric vehicles industries. Therefore, to achieve rapid sinter bonding technology in minutes even under low compression pressure to be applied to the real manufacturing process, the enhancement of sinter-bondability and fast bonding by the combined action of a reduction solvent and efficient carboxylic acid was evaluated in this study [29]. As a criterion for achieving the enhanced bondability, we selected the time for forming the sintered Cu joint corresponding to the shear strength of 15 MPa, which was set as the required minimum shear strength in a related consortium [34].

2 Experimental Procedure

2.1 Paste Preparation

A bimodal mixture of Cu particles was mixed from micrometer-sized Cu particles (CUSP20, JoinM) and submicrometer-sized Cu particles, that were supplied by JoinM (Nonsan-city, Korea) and Epsilon Epowder (Seongnam-city, Korea), respectively. First, these Cu particles were mixed with ethanol at a weight ratio of 6 (micrometer-sized particles):4 (submicrometer-sized particles) and subsequently ultra-sounded for 5 min to even distribute the Cu particles. Then, the ethanol of this Cu particles was dried for 10 h at 25 °C in a low-vacuum chamber. Upon drying, the mixed Cu particles were manually mixed with a polyol-based reducing solvent (EW-10, Epsilon Epowder) at the particle-to-solvent weight ratio of 1:0.15; this paste was named "paste 1". To further increase the reducibility in the Cu paste formulation, succinic acid (≥ 99.0%, Daejung Chemicals & Metals) and ascorbic acid (≥ 99.0%, Sigma-Aldrich) was pre-mixed with the polyol-based reducing solvent, at 15% of the solvent weight; these pastes were named, as "paste 2" and "paste 3" respectively.

2.2 Sinter Bonding Procedure

To prepare a sandwich sample for bondability studies, a dummy Cu die (volume, 3 mm × 3 mm × 1 mm) was sinter-bonded to a dummy Cu substrate (volume, 10 mm × 10 mm × 1 mm). First, the Cu dummies were polished with a 2000-mesh sandpaper. Then, they were etched for 1 min with an etchant (90 mL ethanol (95%, Korea Alcohol Industrial)/10 mL sulfuric acid (98%, Daejung Chemicals & Metals)) before the Cu samples were fabricated.

After rinsing with ethanol and drying with air blowing, the prepared Cu pastes were stencil-printed onto the center surface of the Cu substrate through a stencil mask with a 3 mm × 3 mm × 0.1 mm slit. Subsequently, the die was aligned and placed on the printed Cu pattern, and this sandwich-structured sample was heated in air up to 300 °C at a heating rate of ~ 27 °C/min with a custom-made thermo-compression bonder. Sintering pressure of 2 MPa was imposed immediately after the temperature reached 200 °C, and the bonding time was measured immediately after the compression began. The compressive pressure was maintained throughout the bonding period. The Cu joint samples were released after bonding for 1–10 min and was air-cooled. Then, the sinter-bonding characteristics were analyzed as a function of the bonding time. The sinter-bonding process is schematically shown in Fig. 1.

2.3 Characterization of Materials and a Formed Bondline

The flowability of the mixed Cu particles was examined using a hall flow test to obtain the mass flow rate by measuring the time taken for 500 g of the powder to fall through a funnel.

The bondabilities of the prepared Cu paste samples were evaluated based on the shear strength values measured at the formed bondlines. The shear strength was defined as the average maximal stress values measured during the testing of ten Cu samples with a shear speed of 200 μm/s at a shear-tip height of 200 μm above the substrate surface. The morphologies of the Cu particles, the microstructures of the formed bondlines, and the fracture surfaces after the shear testing were examined by high-resolution field-emission scanning electron microscopy (SEM, SU8010, Hitachi). The bondlines for observation were prepared by cross-sectional polishing after mounting the samples, and the microstructure images were acquired in the back-scattered electron (BSE) mode, to easily distinguish the different heterogeneous phases (e.g., Cu oxides). The phase identification in the bondlines of the sintered Cu

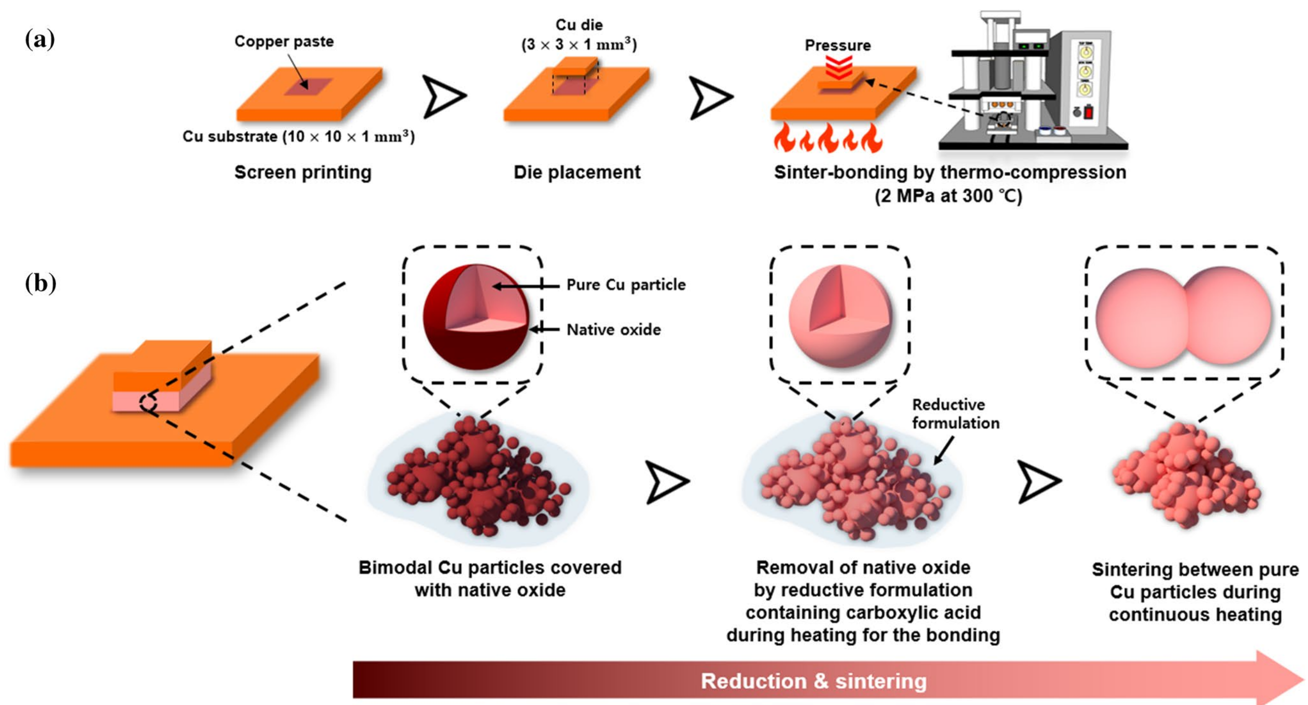

Fig. 1 Schematic scenario of **a** a sinter-bonding process and **b** transformation sequence of Cu particles in the printed sinter-bonding paste during the process

joints was also analyzed by x-ray diffraction (XRD, DE/D8 Advance, Bruker). In order to understand the thermal properties (weight change and heat flow status) vis-a-vis the Cu pastes sinterability, a thermogravimetric–differential thermal analysis (TG–DTA) was also conducted by heating to 500 °C in the air at a heating rate of 20 °C/min. with a Shimadzu DTG-60 model.

3 Results and Discussion

3.1 Particle Properties

Figure 2 shows the morphologies and sizes of the Cu particles used in this study. The micrometer-sized Cu particles were irregularly spherical (average size: 1.86 µm) and had rough surfaces. Meanwhile, the sub-micrometer-sized Cu particles were also irregularly spherical, but their surfaces were relatively smooth. The average size of the latter was relatively small at approximately 340 nm, but they were scarcely aggregated. The mass flow rates of the mixed particles flowing through the funnel were measured as 12.45 and 35.29 g/s for orifices with diameters of 18 and 28 mm, respectively. When comparing the measured rates of sugar with identical diameters, the rates of the mixed particles were approximately 22% of that of sugar.

3.2 Microstructures by Sinter-bonding

Figure 3 shows the cross-sectional BSE images of the upper and lower bondlines, sinter-bonded for different bonding times (1, 3, 5 and 10 min) with paste 1. In short, the microstructural densities of the bondlines consistently showed an increased density with the increase of bonding time; in particular, the increase of bonding time from 1 to 3 min resulted in the most significant increase in joint density. Based on the differences in phase change, the surface oxidation was observed for both types of Cu particles in the 1-min-bonded sample (Fig. 3a). The oxidation severely propagated in the 3-min-bonded sample (Fig. 3b), transforming the thick surfaces of 2-µm-sized Cu particles and a significant number of 340-nm-sized Cu particles into Cu oxide. Therefore, the porous Cu bondline structure in the air at 300 °C rapidly oxidized as the bonding time increased.

As the bonding time increased to 5 min (Fig. 3c), more oxide phases were visible with slightly enhanced densification, transforming most of the 340-nm-sized Cu particles into Cu oxide; Cu cores, consisting of the 2-µm-sized Cu particles, were observed as islands in the Cu oxide matrix. Finally, the 20-min-bonded sample (Fig. 3d) exhibited further oxidized states, together with the additional removal of large voids. In summary, the oxidation rapidly proceeded for 3 min, and then tapered for bonding times longer than 3 min. These results implied that the bondline oxidation was

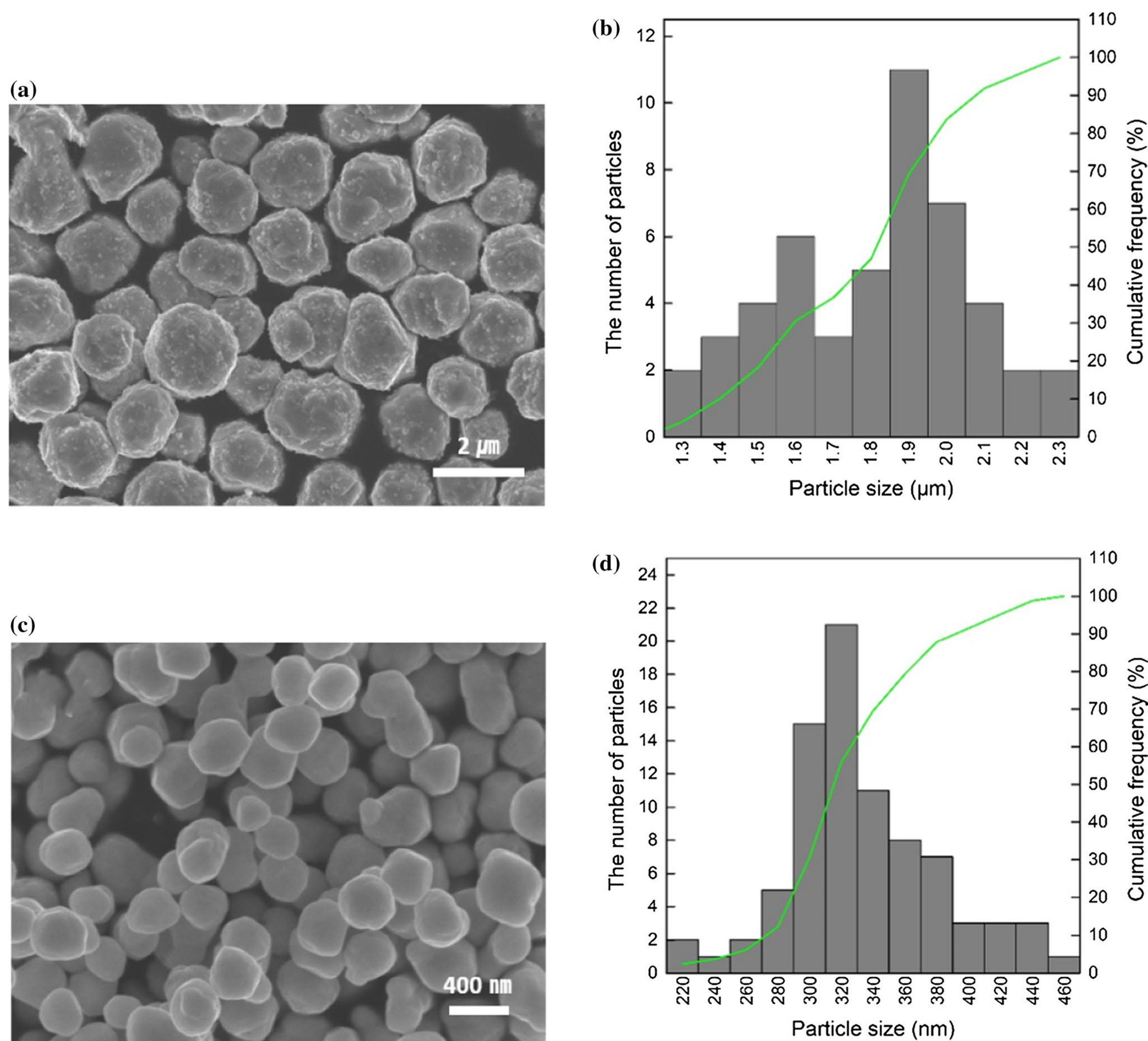

Fig. 2 **a**, **c** Morphologies and **b**, **d** histograms of Cu particles of two types: **a**, **b** micrometer-sized particles and **c**, **d** submicrometer-sized particles

suppressed after the bondline became denser due to the lack of oxygen penetration; the oxidation vigorously proceeded only, if the density was low.

Cross-sectional BSE images of the upper and lower bondlines formed using paste 2 are shown in Fig. 4. In the 1-min-bonded sample (Fig. 4a), a relatively high-density structure was observed with an irregular distribution of voids but lacked the identification of clear Cu oxides phases. The relatively dense microstructure was also obtained equally at the upper and lower Cu/bondline interfaces. As the bonding time increased to 3 min (Fig. 4b), the bondline density increased significantly, and the distribution of voids became relatively regular and periodical. In the same manner, the microstructural densities at the interfaces also clearly improved. When the bonding time approached 5 min (Fig. 4c), a representative bondline structure with a near-full density was observed. This microstructural transition was completely different from that for paste 1, which did not contain succinic acid. The near-full density bondline at 10-min bonded sample was identical with the 5-min-bonded sample, and thus not shown here.

Cross-sectional images of the bondlines fabricated using paste 3 are displayed in Fig. 5. The 1-min-bonded sample (Fig. 5a) showed a relatively high-density structure without oxide phase, with a more regular distribution of voids compared to "paste 2 in Fig. 4a. The degrees of densification at

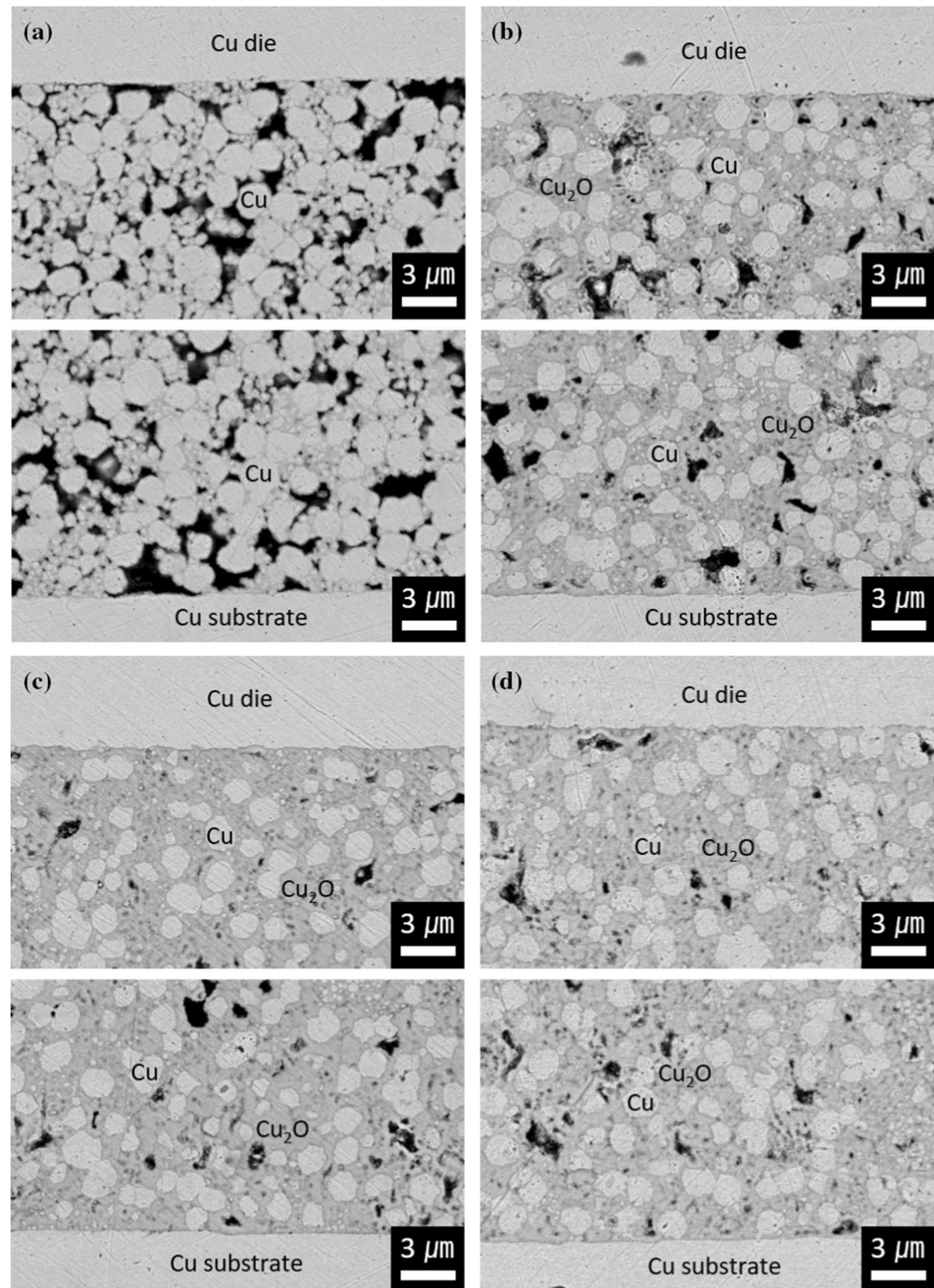

Fig. 3 Cross-sectional BSE images of the bondline at the upper and lower interfaces, for samples that were sinter-bonded using paste 1 under 2-MPa compression at 300 °C in air, for different times: **a** 1 min, **b** 3 min, **c** 5 min, and **d** 10 min

the upper and lower interfaces were identical. Nevertheless, contours of the added 1.86 μm and 340 nm Cu particles were observed, and thus, indicated insufficient sintering degree between the Cu particles. As the bonding time increased to 3 min (Fig. 5b), the bondline density increased when the wide gaps between particles and partial coarsening of the sintered aggregates began to be filled, and thus improving the densities at the joint interfaces with the substrates. The gap-filling and the coarsening of sintered aggregates proceeded further to achieve the near-full density structure when the bonding time increased to 5 min (Fig. 5c). The improved microstructural transition, obtained from the paste 3 containing ascorbic acid (Fig. 5), was similar to that for paste 2 containing succinic acid (Fig. 4); these improved pastes 2 and 3 showed a clear and improved difference from those microstructural properties shown in paste 1 which did not include the two carboxylic acids.

To analyze the oxidation states in the bondlines formed during the sinter bonding, a sintering for 3 min at 300 °C in the air was performed on the large-area printing of Cu pastes on the glass plate, and XRD analysis was conducted on these sintered Cu films. Figure 6 presents the XRD

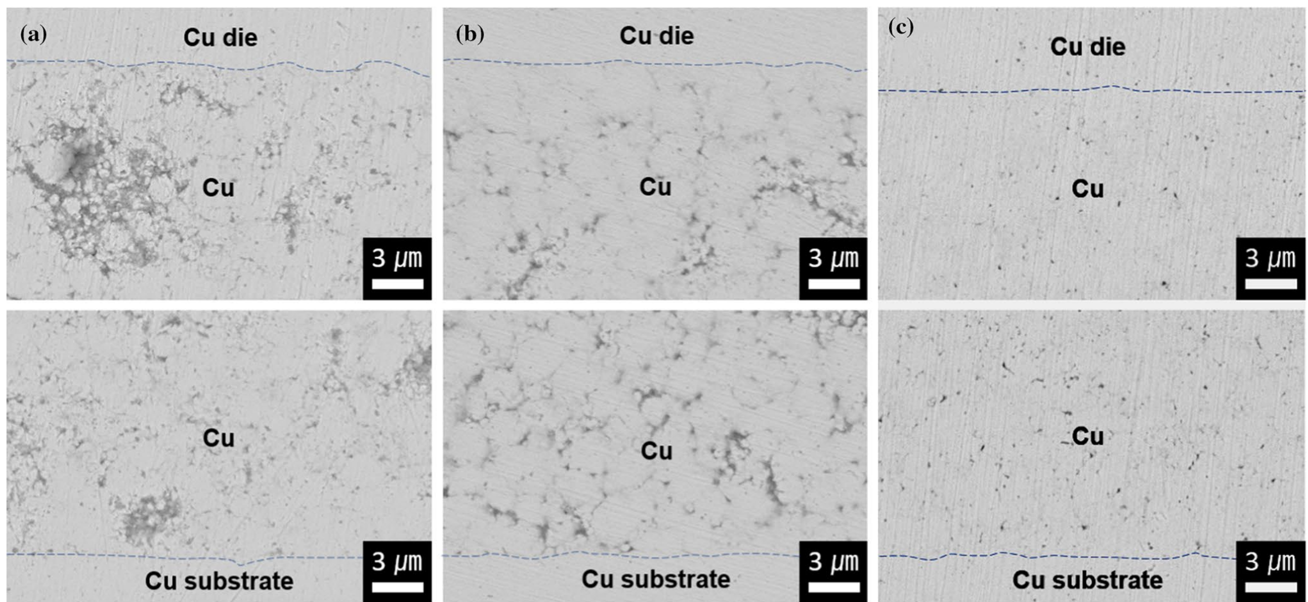

Fig. 4 Cross-sectional BSE images of the bondline at the upper and lower interfaces, for samples that were sinter-bonded using paste 2, for the compression under 2 MPa at 300 °C in air, for different times: **a** 1 min, **b** 3 min, and **c** 5 min

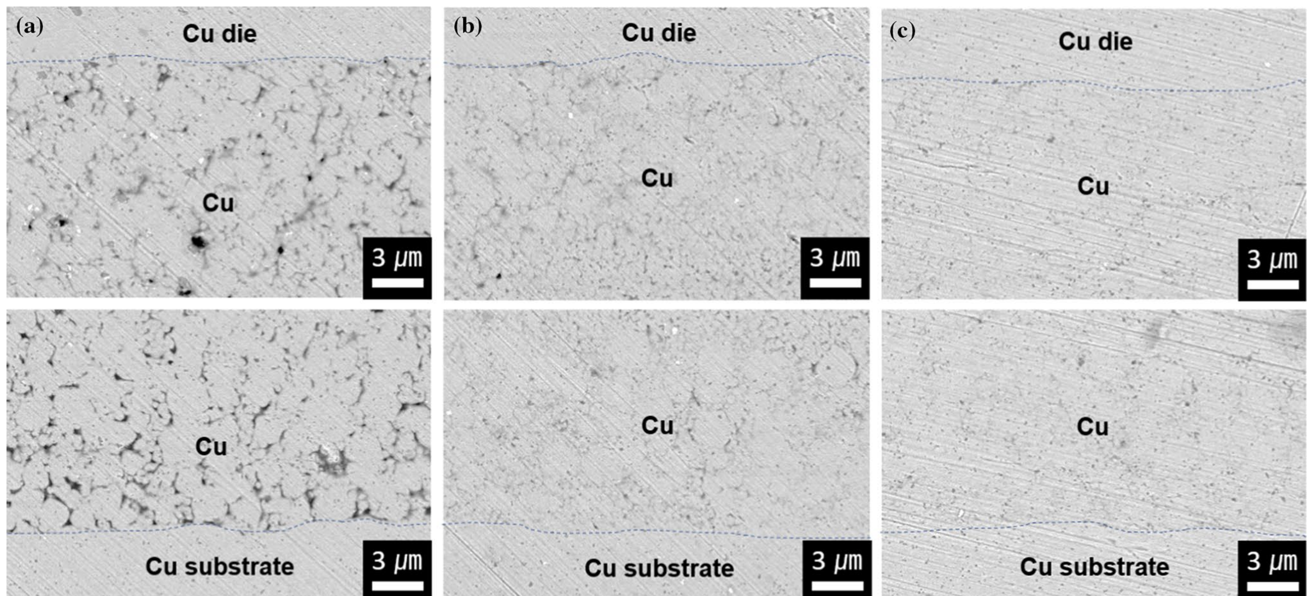

Fig. 5 Cross-sectional BSE images of the bondline at the upper and lower interfaces, for samples that were sinter-bonded using paste 3, for the 2-MPa compression at 300 °C in air, for different times: **a** 1 min, **b** 3 min, and **c** 5 min

results obtained after the pressureless sintering of these Cu pastes. For the paste 1 containing only the polyol-based solvent without any carboxylic acid, the main diffraction peak of Cu_2O phase was clearly indexed, indicating the oxidation of Cu particles during the air-sintering. However, this main peak of Cu_2O decreased in the sample using the paste 2 containing succinic acid, implying suppression of the Cu oxidation. Finally, this main peak of Cu_2O disappeared in the Cu sample formed from paste 3 containing ascorbic acid; the absence suggested that the addition of ascorbic acid (paste 3) is more effective than succinic acid (paste 2) to reduce the Cu oxides in the air at 300 °C. Overall, the Cu pastes containing carboxylic acids (paste 2 and 3) provided an effective sintering by

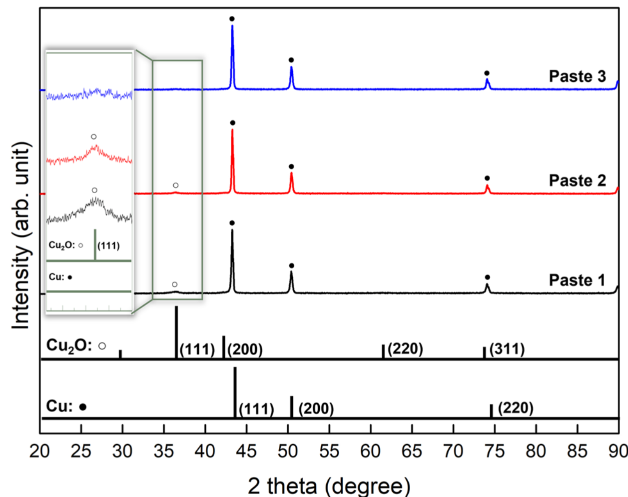

Fig. 6 X-ray diffraction patterns obtained after the sintering of different pastes for 3 min at 300 °C in air. Note that the peaks corresponding to the (111) plane of the Cu_2O phase were magnified in the left inset box

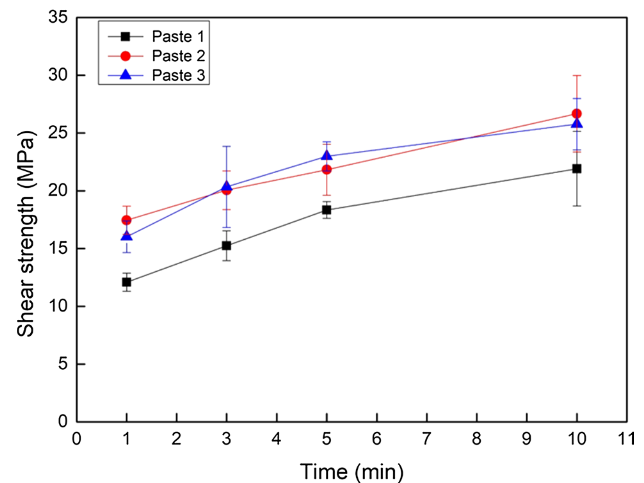

Fig. 7 Shear strengths of the bondlines sinter-bonded under 2 MPa at 300 °C in air, for different paste types and different bonding times

suppressing or reducing the oxidation of Cu particles to promote sintering.

If a pressure of 2 MPa was applied during the bonding stage, sintering in the bondline using pastes 2 and 3 proceeded effectively to realize microstructures corresponding to those shown in Figs. 4 and 5. However, in the absence of these carboxylic acids, the Cu_2O oxide formed on the particle surface interrupted the neck formation between Cu particles and the corresponding diffusion of Cu atoms through these necks [35]. Thus, the rapid increase of the bondline density through effective sintering could not accomplished, as shown in Fig. 3 (paste 1), when the oxidation of Cu particles obviously proceeded.

3.3 Shear Strength of Formed Bondlines

Figure 7 shows the average shear strength values for the pressure-sintered Cu joints formed at sintering pressures of 2 MPa at 300 °C, for various times; these results are shown for the three different Cu pastes. Although the strength of all sintered Cu joints increased proportionally with an increase of bonding time, joints from pastes 2 and 3 exhibited higher strengths than those from paste 1, with each increment of bonding times. For example, shear strength from sintered Cu joints from pastes 2 and 3 exceeded 15 MPa for sintering time as short as 1 min. In addition, the sintered Cu joints from pastes 2 and 3 increased to the highest level at 26.7 MPa and 25.8 MPa, respectively, after 10 min of bonding. Hence, these results suggested that the sinter-bonding time can be shortened to 3 min for pastes 2 and 3 containing carboxylic acid to achieve the minimum level of 15 MPa, specified earlier in this research [34].

In comparison, the sintered Cu joints from paste 1 showed low densification after 1-min of bonding and severe oxidation after 3-min bonding. Nevertheless, the polyol solvent itself in paste 1 was sufficient to remove the native Cu oxides to allow sintering between Cu inter-particles and substrate surface; they further densified the sintered Cu joints to elevate the shear strengths to between 12.1 MPa to 15.2 MPa at the sintering time of 1 and 3-min respectively.

3.4 Fractography of Bondlines

The SEM images of fracture bondlines after the shear testing are shown for the different Cu pastes and bonding times in Fig. 8. All observed fractography exhibited a cohesive failure mode, i.e., the fractures occurred within the bondlines, implying that the Cu pastes sintered well with the upper Cu dummy dies and lower Cu substrates with a combination of the reduction polyol solvent and carboxylic acid.

Compared to sintered Cu joints from paste 2 and 3, the fracture surfaces of sintered Cu joints from paste 1 had a relatively less dense structure for equivalent bonding time. For example, a porous microstructure was observed for the sintered Cu joint formed with a 1-min-bonding time because of its insufficient sintering. When the bonding time was increased to 3 min, coarse structures were observed, but tiny oxide particles that were not sinterable were also observed. These Cu oxide particles prevented effective sintering despite increasing bonding time to 5 min or 10 min; this sintering failure yields less dense structures and brittle fracture surfaces with slight plastic deformation.

On the other hand, the fracture surfaces formed by paste 2 showed a fairly sintered structure with few local cracks after 1 min of bonding. As the bonding time increased to 3 min, shear bands developed in the well-sintered regions. A fully

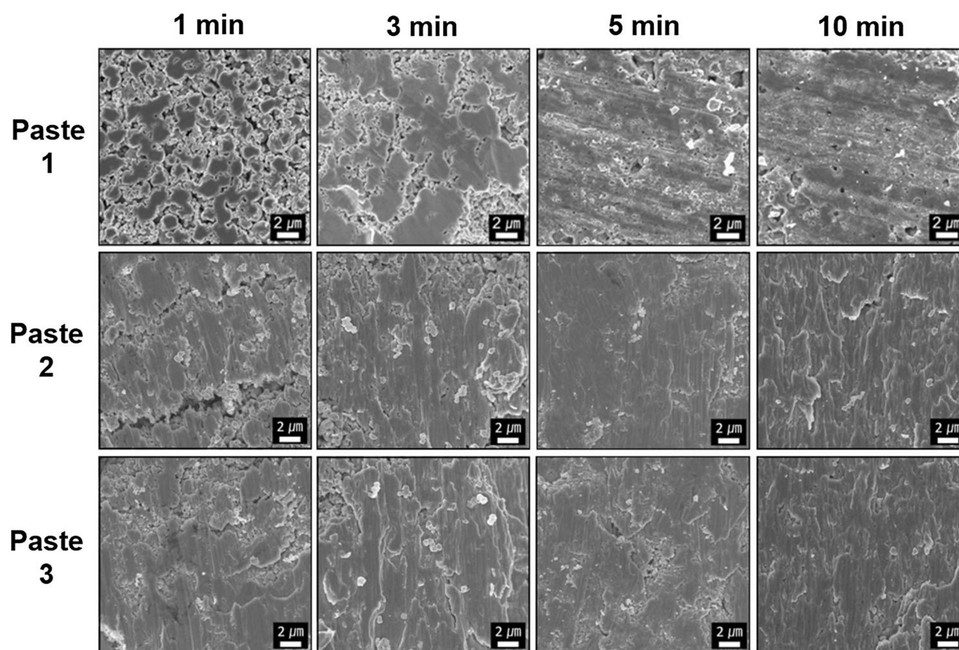

Fig. 8 Fracture surface SEM images of the formed bondlines, for samples sinter-bonded using different pastes, under 2 MPa at 300 °C, for different bonding times

sintered microstructure was finally observed on most surface regions when the bonding time increased to 5-min-bonding. After 10 min of bonding, the fracture surface exhibited a plastically deformed microstructure by elongation, similar to that manifested by a well-bonded metallic bondline [33, 36].

Finally, the fractography of the samples prepared using paste 3 were similar to the sequential results of sintered Cu joints from paste 2. In addition, the observed fractography results corresponded with the bondline microstructure results shown in Figs. 3, 4 and 5. Based on Figs. 3, 4, 5 and 6, the degree of sintering correlated with the measured shear strength values and the cohesive fracture surfaces. Therefore, sinter bonding using pastes 2 and 3 demonstrated enhanced sinterability and increased density improvement in the bondlines formed. The reduction of Cu oxide phases in the sintered Cu joints using pastes 2 and 3 also suggests a bonding interface with excellent thermal conductivity and high-temperature sustainability.

3.5 Thermal Analysis and Sinter-Bonding Mechanisms

The TG–DTA results for the Cu pastes sintered in the air are shown in Fig. 9. All three Cu pastes exhibited a weight decrease at temperatures above 150 °C, and exothermic curves as the temperatures approached 200 °C. However, the main peak temperatures of the exothermic curves formed by sintering between the particles were entirely different for the different pastes: 240, 270, and 275 °C for pastes 1, 2, and 3, respectively. Hence, the addition of carboxylic acids delayed the main sintering temperature.

Figure 9 also shows that the end of the weight decrease and the beginning of the weight increase by Cu oxidation differed for pastes 1, 2, and 3, at corresponding temperatures of 230, 250, and 265 °C, respectively. These results implied that the organic remnants in the Cu pastes containing carboxylic acid reduce or delay the Cu oxidation. Their differences in the main peak temperatures of the exothermic curves could be attributed to these remnants. These organic remnants, which protected the Cu particles from oxidation, widened the sintering range and the overall degree of sintering. The enhanced sintering degrees and delay in the Cu oxidation were confirmed by the corresponding increase in the areas under the exothermic curves for temperatures up to 300 °C (note that the Y-axis ranges of heat flow are different from each other). The surviving exothermic curves for temperatures exceeding 300 °C were primarily attributed to sintering between oxidized particles; the degree was the highest for paste 1.

Since the results shown in Fig. 9 were obtained under pressureless conditions, the results for the actual pressure-assisted (compressive) sinter bonding would be slightly different. It is anticipated that the oxidation tendency would be suppressed, and the sintering degree would significantly improve by accelerating the sintering process, especially for Cu pastes 2 and 3 containing carboxylic acid. Although Cu particles may re-oxidize in the air at high temperatures even after in situ reduction, oxidation can be significantly suppressed if the Cu particles are rapidly sintered into a dense microstructure with the assistance of compressive pressure.

Besides oxide removal from the Cu particle surfaces and delayed oxidation due to the inclusion of carboxylic acid, Cu particle rearrangement contributed to the rapid sinter

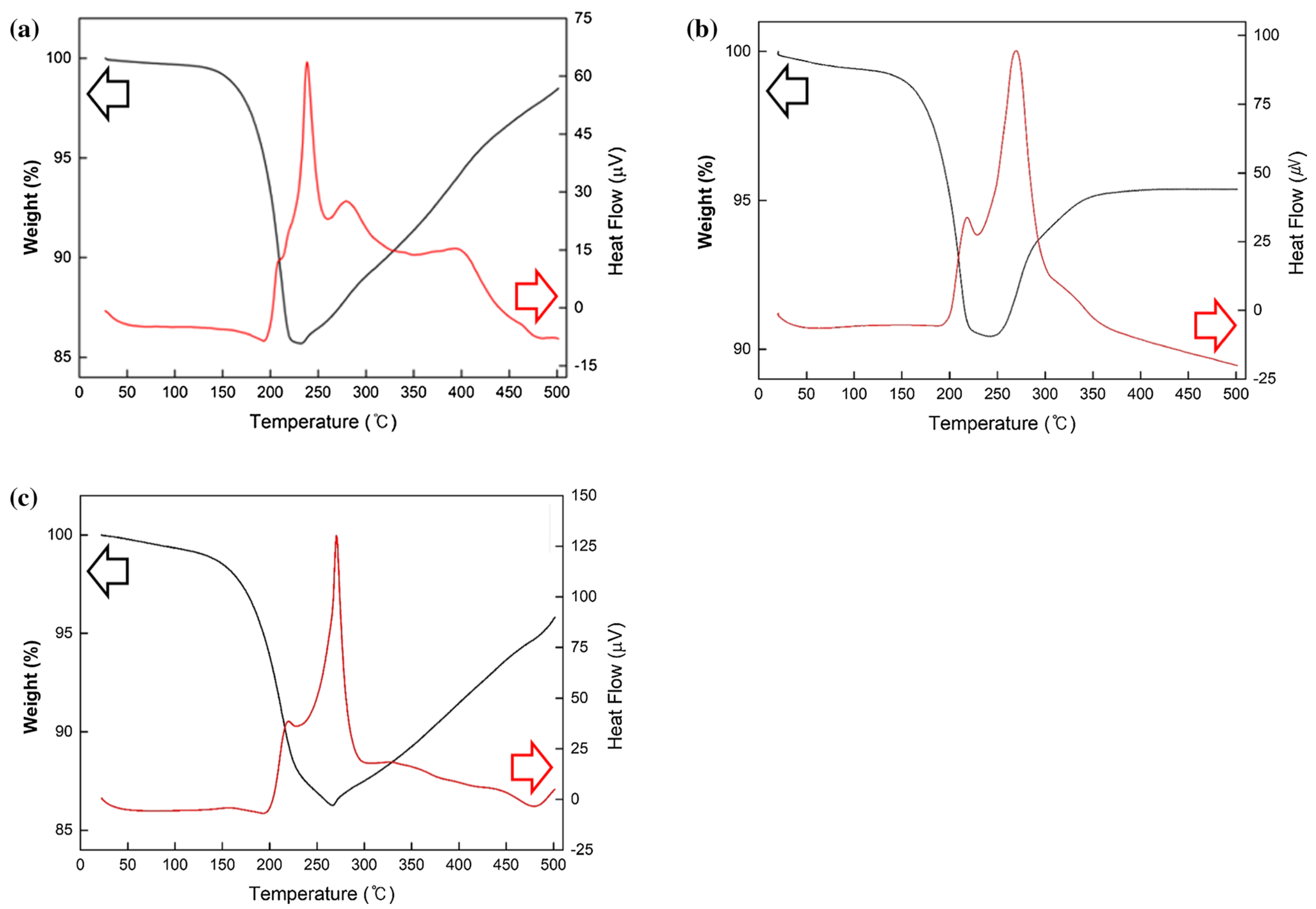

Fig. 9 TG–DTA results during heating to 500 °C for the prepared **a** paste 1, **b** paste 2, and **c** paste 3

bonding [37, 38]. The particle rearrangement is the slow movement of particles in the bondlines, heading for stress-free voids to escape the fraction between particles under constant compressive stress. Optimal positioning of the particles naturally proceeded by rearrangement, which absorbed the surface roughness at the upper and lower Cu interfaces, which was essential to induce the bonding integrity [39].

4 Conclusions

The pressure-assisted sintered Cu joints were demonstrated for die-attachment application in the air using pastes made from bimodal-sized Cu particles with the addition of carboxylic acids to the polyol-based solvent. The Cu particle sizes were 1.86 μm and 340 nm, while the compressive pressure was 2 MPa. The addition of carboxylic acids, i.e. succinic acid or ascorbic acid, into the Cu pastes improved the reduction propensity and sinter-bondability at 300 °C significantly. Consequently, these remnant organics from the carboxylic acids in the used polyol-based reducing system were effectively accelerating the sintering process together while delaying the Cu reoxidation. Accordingly, the shear strengths of the sintered Cu joints exceeded 15 MPa, similar to the required minimum shear strength, despite the significantly short bonding of 1 min. Furthermore, the bondlines in the sintered Cu joints with 3-min bonding showed high purity Cu phase with the minimal oxidation even in the air-bonding. Furthermore, when the bonding time increased to 5 min, a near-full-density bondline structure were formed. The obtained results imply that the combination of effective reducing agents is crucial for enhancing the sinterability for the Cu joint. Consequently, the short sintering time of these carboxylic acid-enhanced Cu pastes provides a guideline for the next-generation sinter-bonding technologies using low-cost Cu particles in the air atmosphere.

Acknowledgements This study was supported by the Research Program (2021-1132) funded by the SeoulTech (Seoul National University of Science and Technology).

Declarations

Conflict of interest On behalf of all authors, the corresponding author states that there is no conflict of interest.

References

1. L.A. Navarro, X. Perpiñà, P. Godignon, J. Montserrat, V. Banu, M. Vellvehi, X. Jordà, IEEE Trans. Power Electron. **29**, 2261 (2014)
2. P.G. Neudeck, R.S. Okojie, L.-Y. Chen, Proc. IEEE **90**, 1065 (2002)
3. F. Roccaforte, P. Fiorenza, G. Greco, R.L. Nigro, F. Giannazzo, F. Iucolano, M. Saggio, Microelectron. Eng. **187–188**, 66 (2018)
4. W.S. Hong, M.S. Kim, C. Oh, Y. Joo, Y. Kim, K.-K. Hong, JOM **72**, 889 (2020)
5. W.S. Hong, M.S. Kim, C. Oh, J. Electron. Mater. **49**, 188 (2020)
6. R.W. Johnson, J.L. Evans, P. Jacobsen, J.R. Thompson, M. Christopher, IEEE Trans. Electron. Packag. Manuf. **27**, 164 (2004)
7. H.S. Chin, K.Y. Cheang, A.B, Metall. Mater. Trans. B **41**, 824 (2010)
8. A. Lis, C. Leinenbach, J. Electron. Mater. **44**, 4576 (2015)
9. B.-S. Lee, S.-K. Hyun, J.-W. Yoon, J. Mater. Sci. Mater. Electron. **28**, 7827 (2017)
10. B.-S. Lee, J.-W. Yoon, Met. Mater. Int. **23**, 958 (2017)
11. H. Zhang, C. Chen, J. Jiu, S. Nagao, K. Suganuma, J. Mater. Sci. Mater. Electron. **29**, 8854 (2018)
12. T.F. Chen, K.S. Siow, J. Alloy. Compd. **866**, 158783 (2021)
13. E.B. Choi, J.-H. Lee, Met. Mater. Int. **27**, 5278 (2021)
14. T. Yamakawa, T. Takemoto, M. Shimoda, H. Nishikawa, K. Shiokawa, N. Terada, J. Electron. Mater. **42**, 1260 (2013)
15. B.H. Lee, M.Z. Ng, A.A. Zinn, C.L. Gan, in *Proceedings of 22nd International Symposium on the Physical and Failure Analysis of Integrated Circuits* (IEEE, Hsinchu, 2015), pp. 102–106
16. J. Zhao, M. Yao, N.-C. Lee, in *Proceedings of 68th Electronic Components and Technology Conference (ECTC)* (IEEE, San Diego, 2018), pp. 557–563
17. T. Ishizaki, R. Watanabe, J. Mater. Chem. **22**, 25198 (2012)
18. Y. Kobayashi, T. Shirochi, Y. Yasuda, T. Morita, Intl. J. Adhes. Adhes. **33**, 50 (2012)
19. J. Kahler, N. Heuck, A. Wagner, A. Stranz, E. Peiner, A. Waag, IEEE Trans. Compon. Packag. Manuf. Technol. **2**, 1587 (2012)
20. Y. Kobayashi, T. Shirochi, T. Maeda, Y. Yasuda, T. Morita, Surf. Interface Anal. **45**, 1424 (2013)
21. Y. Kobayashi, Y. Abe, T. Maeda, Y. Yasuda, T. Morita, J. Mater. Res. Technol. **3**, 114 (2014)
22. T. Ishizaki, R. Watanabe, R&D Rev. Toyota CRDL **46**, 21 (2015)
23. X. Liu, H. Nishikawa, Scr. Mater. **120**, 80 (2016)
24. K.S. Siow, Y.T. Lin, J. Electron. Packag. **138**, 020804 (2016)
25. Y. Gao, H. Zhang, W. Li, J. Jiu, S. Nagao, T. Sugahara, K. Suganuma, J. Electron. Mater. **46**, 4575 (2017)
26. X. Liu, H. Nishikawa, J. Mater. Sci.: Mater. Electron. **28**, 5554 (2017)
27. K. Mohan, N. Shahane, P.M. Raj, A. Antoniou, V. Smet, R. Tummala, in *Proceedings of 2017 Applied Power Electronics Conference and Exposition (APEC)* (IEEE, Tampa, 2017), pp. 3083–3090
28. D. Ishikawa, H. Nakako, Y. Kawana, C. Sugama, M. Negishi, Y. Ejiri, S. Ueda, B.N. An, H. Wurst, B. Leyrer, T. Blank, M. Weber, in *Proceedings of 7th Electronic System-Integration Technology Conference (ESTC)* (IEEE, Dresden, 2018), pp. 1–10
29. Y. Mou, Y. Peng, Y. Zhang, H. Cheng, M. Chen, Mater. Lett. **227**, 179 (2018)
30. Y. Mou, J. Liu, H. Cheng, Y. Peng, M. Chen, JOM **71**, 3076 (2019)
31. D. Ishikawa, B.N. An, M. Mail, H. Wurst, B. Leyrer, T. Blank, M. Weber, S. Ueda, H. Nakako, Y. Kawana, in *Proceedings of 2019 International Conference on Electronics Packaging (ICEP)* (IEEE, Niigata, 2019), pp. 167–172
32. Y. Yamada, K. Hasegawa, Y. Ikeda, K. Katagiri, H. Kayou, Y. Sano, Microelectron. Reliab. **100**, 113316 (2019)
33. J. Li, Q. Liang, T. Shi, J. Fan, B. Gong, C. Feng, J. Fan, G. Liao, Z. Tang, J. Alloy. Compd. **772**, 793 (2019)
34. Die-attach material requirement specification. (DA5, 2021). https://www.infineon.com/dgdl/DA5_customer_presentation_1612016.pdf?fileId=5546d4616102d26701610905cfde0005. Accessed 20 August 2021
35. Y. Zuo, S. Carter-Searjeant, M. Green, L. Mills, S.H. Mannan, Mater. Lett. **276**, 128260 (2020)
36. Y. Peng, Y. Mou, J. Liu, M. Chen, J. Mater. Sci.: Mater. Electron. **31**, 8456 (2018)
37. B. Ratzker, M. Sokol, S. Kalabukhov, N. Frage, J. Eur. Ceram. Soc. **38**, 1271 (2018)
38. M.I. Kim, E.B. Choi, J.-H. Lee, J. Mater. Res. Technol. **9**, 16006 (2020)
39. M. Wang, Y. Mei, X. Li, R. Burgos, D. Boroyevich. G.-Q. Lu, Mater. Lett. **228**, 327 (2018)

Publisher's Note Springer Nature remains neutral with regard to jurisdictional claims in published maps and institutional affiliations.